The International Journal of Advanced Manufacturing Technology
https://doi.org/10.1007/s00170-026-17867-3

ORIGINAL ARTICLE

Effect of flux composition on metal transfer characteristics in rutile-type flux-cored arc welding

Dang Khoi Le[1] · Shinichi Tashiro[1] · Kieu Anh Duong Nguyen[1] · Quang Ngoc Trinh[1,2] · Tetsuo Suga[1] · Naoki Sawamura[3] · Kazuhiro Fukuda[3] · Shuji Sasakura[3] · Patricio Fernando Mendez[4] · Anthony B. Murphy[5] · Van Hanh Bui[2] · Manabu Tanaka[1]

Received: 1 October 2025 / Accepted: 9 March 2026

Abstract

This study clarified the effects of flux composition on metal transfer characteristics in rutile-type Flux-Cored Arc Welding (FCAW). Seven prototype wires with varying TiO_2, SiO_2, and CaF_2 contents in the flux were tested at three currents (220–280 A) under Ar-20%CO_2 shielding. The Droplet Diameter (DD), which is important for arc stability, is proportional to the ratio of the Wire Feed Speed (WFS) and the Metal Transfer Frequency (MTF), which are primarily governed by the energy and force balances, respectively. The WFS depended on the iron content in the flux, was almost independent of the TiO_2, SiO_2, and CaF_2 content, and increased linearly with current. Increasing the CaF_2 content reduced the MTF sharply from 86.9 to 34.0 Hz at 220 A due to either the strong recoil pressure caused by vaporization from CaF_2 or strong arc pressure by the high specific heat of CaF_2 plasma. These pressures pushed the droplet upward, hindering droplet detachment. TiO_2 showed a slight increase in MTF with TiO_2 content (for example, 162.5 to 170.3 Hz at 280 A). SiO_2 showed a significant increase in MTF with SiO_2 content, especially at 280 A (170.3 to 222.9 Hz), probably due to slag-metal reactions increasing the oxygen concentration in the droplets, leading to a lower surface tension; the effect is stronger for SiO_2 because its basicity lower than that of TiO_2. Thus, the flux composition affected the MTF much more strongly than the WFS, so that the DD was inversely proportional to MTF. Consequently, it was found that the DD depended strongly on flux composition through variations in the physical properties.

Keywords Flux-cored arc welding · Metal transfer · Recoil pressure · Specific heat · Surface tension · Flux column

1 Introduction

Flux-Cored Arc Welding (FCAW) is an arc welding process using an electric arc ignited between a continuously fed tubular wire and base metal to generate heat for welding [1]. The arc heat melts the wire, forming a molten droplet at the tip of the wire. This droplet falls through the arc plasma to reach the base metal, forming a weld pool [1]. Shielding is provided either by the flux inside the wire alone or in combination with an external shielding gas. FCAW is widely used in various industrial fields due to its versatility, high deposition rates, high welding speed, and ease of operation [1]. Part of its versatility comes from the unique structure of the wire, which enables the inclusion of various powder elements within the metal sheath to suit specific welding demands. Based on the composition of the internal flux, flux core wires are classified into sub-groups: metal-type flux core wire (metal core wire) [2], basic-type flux core wire

✉ Shinichi Tashiro
tashiro.shinichi.jwri@osaka-u.ac.jp

✉ Quang Ngoc Trinh
ngoc.trinhquang@hust.edu.vn

[1] Joining and Welding Research Institute, The University of Osaka, Osaka, Japan

[2] Hanoi University of Science and Technology, Hanoi, Vietnam

[3] Kobe Steel, Ltd, Kanagawa, Japan

[4] University of Alberta, Edmonton, Canada

[5] CSIRO, Manufacturing, Lindfield, Australia

Published online: 26 March 2026

(basic wire) [3], and rutile-type flux core wire (rutile wire) [4].

Metal core wire, whose flux mainly consists of iron powder, is commonly used in Metal-Cored Arc Welding (MCAW), which is a kind of FCAW process. A basic wire, derived from Shielding Metal Arc Welding (SMAW) slag systems with limestone and fluorspar, is widely used. The basic wire improves metal cleanliness by reducing the oxygen, hydrogen, and sulfur contents. It offers excellent mechanical properties for structural steel, but its difficulty in achieving spray transfer (where the Droplet Diameter (DD) is smaller than the wire diameter) has traditionally required positional welding to utilise short-circuiting transfer (where the molten droplet reaches the weld pool while still attached to the wire). This results in some spatter and potential lack-of-fusion defects or cold laps [5]. To overcome the limitations of the basic wire, the rutile wire, primarily composed of titanium dioxide (TiO_2), was developed. Rutile wire provides flexible control over slag melting point and viscosity, along with a good arc stability [1, 5]. In addition, flux additives (minor components in the flux) can be added for specific purposes, such as slag formation (SiO_2, TiO_2, CaO, FeO, MgO, etc.), improving arc stability (alkali elements, rare earth), and decreasing hydrogen content in molten metal (CaF_2, $CaCO_3$). However, rutile wire has limitations such as producing an overly fluid slag and promoting globular metal transfer (where DD is larger than the wire diameter [1, 6]) [5]. Notably, DD influences arc stability, spatter formation, and weld bead appearance [7, 8], which are among the key factors in evaluating welding performance and productivity. Furthermore, heat-transfer-based modeling of Gas Metal Arc Welding (GMAW) has demonstrated that droplet size and transfer mode affect droplet temperature [9], particularly the droplet surface temperature. This affects the fume formation [9, 10]. Mendez et al. [9] suggested that the surface temperature at the electrode tip rises as droplet size increases. Smaller droplets lead to reduced metal vaporization; consequently, spray transfer or pulsed-current welding produces less fume. Nevertheless, aside from improving the deposition rate of GMAW, factors such as penetration, slag removability, and bead shape have been important since the introduction of flux core wire [5]. As a result, most FCAW studies have focused on these aspects, with few directly addressing Metal Transfer Frequency (MTF) and DD quantitatively.

Izutani et al. [6] qualitatively classified metal transfer modes in FCAW for rutile wire by using a High-Speed Video Camera (HSVC). They reported that the metal transfer mode changed from short-circuiting to streaming transfer (elongated molten droplet like a long tail) modes with increased welding current in Ar-20%CO_2 and 100%CO_2 shielding gases. The primary purpose of adding components as TiO_2 or SiO_2 is for slag formation, but these also have secondary effects. Li et al. [11] reported that the addition of SiO_2 can reduce the surface tension of the molten pool compared with TiO_2. It is expected that a similar effect may be observed in molten droplets when SiO_2 is added. Based on the static force balance theory [12], the reduction of surface tension enhances MTF. In addition, Trinh et al. [13] carried out spectral visualizations using bandpass filters to further diagnose arc behavior by examining the distributions of titanium, iron, and argon in plasma. The filters, designated Ti I (568.0 nm), Fe I (540.0 nm), and Ar I (695.5 nm), each had a full width at half maximum of 10.0 nm. They found that the central plasma consisted of a mixture of titanium and iron vapors (titanium and iron plasmas, respectively), which enhanced arc plasma's electrical conductivity. As a result, the current density under the bottom of the molten droplet increased, leading to an increase in arc pressure beneath the droplet, hindering droplet detachment. As in the TiO_2 case, added alkali elements (sodium) altered the arc characteristics such as electrical conductivity [14]. Because sodium has a much lower ionization potential than titanium (5.1 eV and 7.9 eV, respectively), the effect of alkali elements on arc stability is expected to be clearer.

Bauné et al. [8] assessed the effects of adding alkali oxides (containing lithium, magnesium, sodium, and potassium) into a basic wire on metal transfer stability and spatter formation compared to commercial basic and rutile wires. They revealed that basic wires containing alkali oxides provided more stable arcs than commercial basic and even rutile wires, while the rutile wire gave a higher MTF than all the basic wires. Supporting this work, Valensi et al. [15] qualitatively demonstrated the CO_2 content causing the transition from globular to spray transfer at the same current using flux core wires. The results showed that adding alkali stabilized the spray transfer at currents up to 330 A through changes in viscosity, even with gas mixtures containing up to 60% CO_2 in argon. In addition, adding a particular sodium content into rutile-type flux altered arc characteristics to vary the forces acting on droplet. These effects stabilized the metal transfer process [16]. The addition of basic components (CaO, $CaCO_3$, CaF_2, and so on) reduced the stability of the arc and metal transfer [5], but they played a role in decreasing the hydrogen content whether originating from manufacturing process or from contamination of the workpiece by oil or other organic substances during welding.

Limestone and fluorspar, the main components of basic-type flux, not only shield the arc from the atmosphere but also inhibit hydrogen pickup in different ways [5]. Bang et al. [17] concluded that slag basicity influenced the hydrogen content in weld metal independently of the fluorine released from the dissociation of added fluorides. Compared to the rutile wire without fluoride, the one with CaF_2 showing a significant effect: when 2.3 mass% CaF_2 was added, the

diffusible hydrogen content decreased from 10.17 to 6.63 mL per 100 g deposited metal and from 7.13 to 3.32 mL per 100 g fused metal [17], corresponding to decreases of approximately 35.0% and 53.5%, respectively. Furthermore, the high ionization potential of fluorides tended to destabilize the arc. In self-shielded FCAW (FCAW-S), Kil et al. [18] showed that slight changes in slag basicity had a minimal effect on hydrogen content, while excessive fluorine vaporization hindered the droplet detachment, resulting in larger droplets and increased spatter. Through thermodynamic calculations and experiments, Matsushita [19] demonstrated that adding 5% of K_3AlF_6, KF, and MnF_3 effectively reduced diffusible hydrogen in steel welded metal by 22–30%, 35–40%, 21–35%, respectively. The addition of 5% K_3AlF_6 proved to be more effective than 10% addition. KF showed greater hydrogen reduction under higher hydrogen partial pressures, although the mechanism remained unclear. Despite extensive research on FCAW, detailed documentation in the public scientific domain regarding how flux composition in rutile wires influences metal transfer characteristics such as MTF and DD which directly affect arc stability remains limited. Therefore, this study aims to systematically and quantitatively clarify the influence of flux composition on MTF and DD under controlled experimental conditions.

In this study, the effect of flux composition on metal transfer characteristics in rutile-type FCAW was investigated. Metal transfer behavior and arc appearance of seven prototype rutile wires with various TiO_2, SiO_2 and CaF_2 contents were compared at three welding currents of 220, 250 and 280 A in Ar-20%CO_2 FCAW. HSVC was employed to capture the metal transfer and arc appearance during welding using the shadowgraph method. The effects of flux composition on metal transfer characteristics were analyzed based on the recorded videos. The physical mechanisms responsible for the observed effects were considered.

2 Experimental methodology

2.1 Materials and welding conditions

Bead-on-plate welding experiments were conducted using mild steel plates (SS400 – JIS 3101) for the rutile-type FCAW process. Seven prototype flux-cored wires (AWS A5.20 E71T-1 C, 1.2 mm diameter) were developed to examine how variations in flux composition influence metal transfer characteristics in FCAW. These included a standard wire (Wire 1: 40.2% TiO_2, 4.5% SiO_2, and without CaF_2), two wires with different TiO_2 contents (Wire 2: 29.7% TiO_2, Wire 3: 20.1% TiO_2), two wires varied SiO_2 contents (Wire 4: 7.2% SiO_2, Wire 5: 9.9% SiO_2), and two wires with different CaF_2 contents (Wire 6: 4.9% CaF_2, Wire 7: 9.7% CaF_2). The detailed chemical compositions of "flux" for experimental wires are provided in Table 1, while their cross-sectional structures are illustrated in Fig. 1.

The welding experiments were carried out using a welding power source (DP-350, OTC Daihen) equipped with a wire feeder, operating in Direct Current Electrode Positive (DCEP) mode. A consistent Contact Tip to Workpiece Distance (CTWD) of 20 mm was maintained throughout all tests. The wire extension was set to 10 mm before each welding run. Welding was performed at a fixed travel speed of 5 mm s^{-1} using a motorized table. This speed is consistent with that used in References [13, 14, 16], thereby ensuring reliable and comparable results. The target welding current levels (I_{out}) of 220 A, 250 A, and 280 A were chosen to investigate the influence of flux composition on metal transfer characteristics in rutile-type FCAW. For each trial, the I_{out} value was obtained from the welding machine panel as an average value of welding current signals after arc cutting. In practice, depending on the type of welding machine, either Wire Feed Speed (WFS) or current is set as the primary control before welding. For welding machine in this study, current (I_{set}) and voltage (U_{set}) were the primary welding conditions. At a given I_{set}, the machine automatically calculated the WFS using manufacturer-specific functions. The values of the WFS were recorded before doing weld, which differed among the consumables used. Arc voltage varied between 27 V and 32 V to maintain a stable arc length. A shielding gas mixture of argon and 20% CO_2 was supplied at a flow rate of 20 L min^{-1}. Figure 2 illustrates the relationship between WFS and the iron content in the flux. (a) at 220 A, (b) at 250 A, and (c) at 280 A. The full set of welding parameters is summarized in Table 2.

2.2 Metal transfer and arc appearance observations

Figure 3 presents a schematic of the experimental setup used to observe metal transfer behavior and arc appearance. A shadowgraph technique was employed, utilizing HSVC (Memrecam

Table 1 Chemical compositions of "flux" for experimental wires (mass%)

	Wire 1 (Standard)	Wire 2 (↓ TiO_2)	Wire 3 (↓↓ TiO_2)	Wire 4 (↑ SiO_2)	Wire 5 (↑↑ SiO_2)	Wire 6 (↑ CaF_2)	Wire 7 (↑↑ CaF_2)
Fe	23.9	43.3	43.8	21.3	18.7	19.0	14.3
TiO_2	40.2	29.7	20.1	40.2	40.2	40.2	40.2
SiO_2	4.5	4.4	4.3	7.2	9.9	4.6	4.7
CaF_2	-	-	-	-	-	4.9	9.7

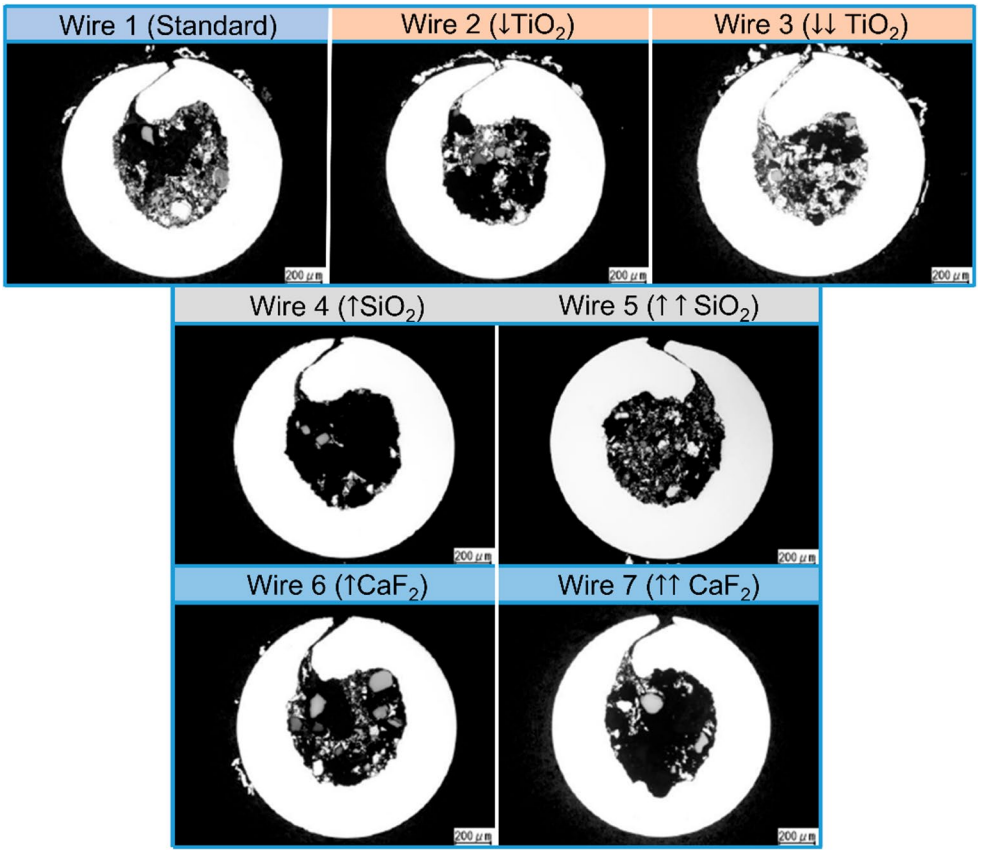

Fig. 1 Observation of experimental wire cross-sectional structures

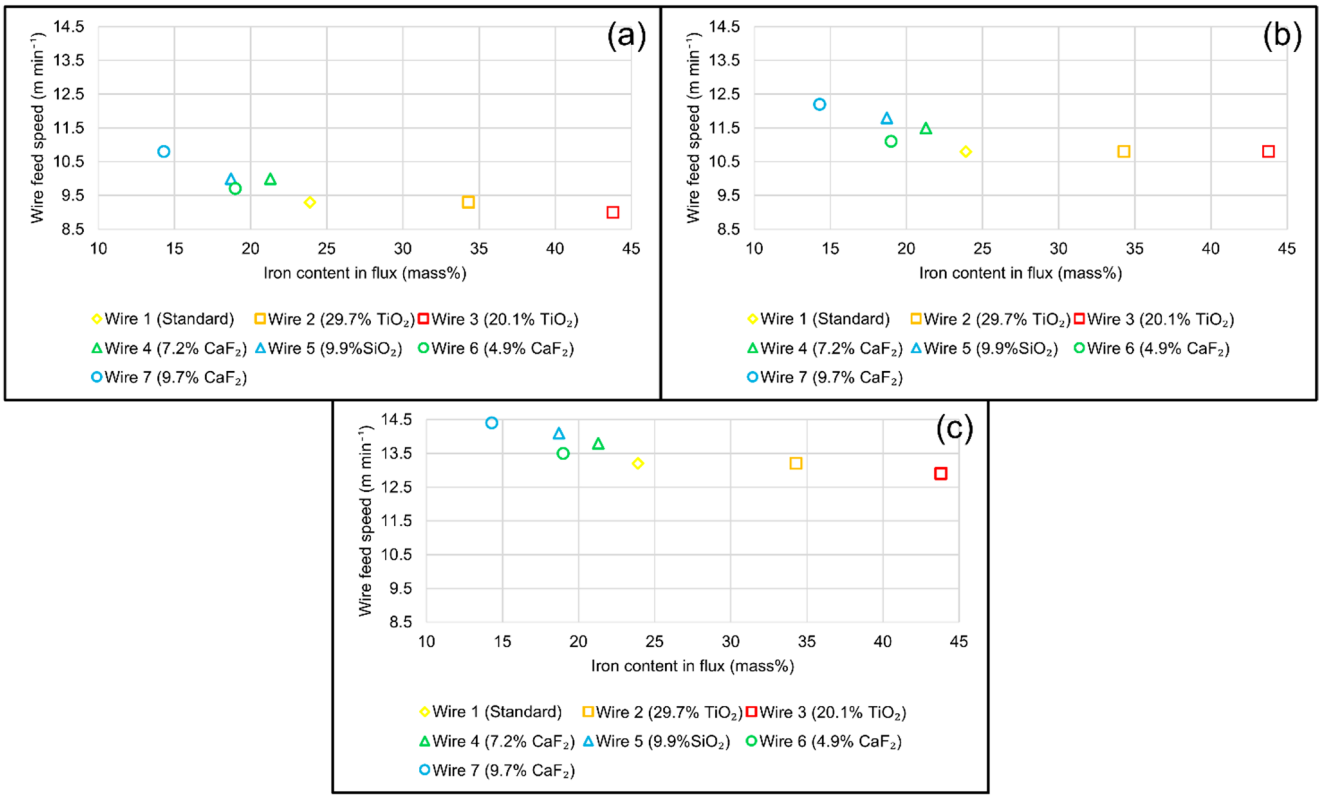

Fig. 2 Wire feed speed as a function of iron content in the flux. (**a**) at 220 A, (**b**) at 250 A, and (**c**) at 280 A

Table 2 Welding conditions

No.	Wire	Current level (A)	I_{set} (A)	U_{set} (V)	I_{out} (A)	U_{out} (V)	WFS (m min^{-1})
1	1		205	27.5	221	27.2	9.3
2	2		205	27.5	223	27.2	9.3
3	3		200	27.5	219	27.3	9.0
4	4	220	215	27.5	223	27.3	10.0
5	5		215	27.5	223	27.3	10.0
6	6		210	27.5	219	27.3	9.7
7	7		225	27.5	222	27.3	10.8
8	1		225	31.0	248	30.3	10.8
9	2		225	31.0	250	30.3	10.8
10	3		225	31.0	250	30.3	10.8
11	4	250	235	31.0	248	30.4	11.5
12	5		240	31.0	254	30.3	11.8
13	6		230	31.0	250	30.3	11.1
14	7		245	31.0	249	30.5	12.2
15	1		260	32.5	277	31.8	13.2
16	2		260	32.5	279	31.7	13.2
17	3		255	32.5	278	31.6	12.9
18	4	280	270	32.5	277	32.0	13.8
19	5		275	32.5	285	32.0	14.1
20	6		265	32.5	278	31.9	13.5
21	7		280	32.5	280	32.2	14.4

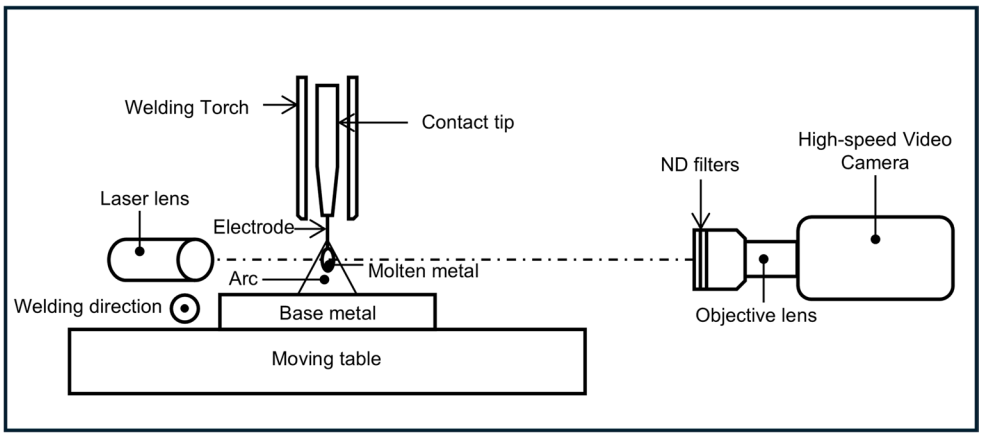

Fig. 3 Schematic of experimental setup for observing the metal transfer behavior and arc appearance using shadowgraph technique

Q1v, Nac Image Technology) equipped with a lens (Micro-NIKKOR, Nikon). The lens featured a 200 mm focal length and a 1:4 focus ratio. A 640 nm laser illumination system was positioned opposite the camera to provide backlighting. Notably, the camera, laser system and the wire were aligned. Additionally, the wire was positioned between the camera and the laser system, with a distance of approximately 150 cm from the wire tip to the camera lens. The camera captured images at 5000 frames per second, with an aperture of f/5.6 and an exposure time of 20 µs. Six Neutral Density (ND) filters: five ND-8 and one ND-4 were used to reduce the radiation and brightness of the arc. While a bandpass filter matching the laser wavelength is commonly used in the shadowgraph technique to further suppress arc radiation, this study relied only on ND filters. This approach enabled the simultaneous visualization of both metal transfer behavior and arc appearance.

3 Results

3.1 Metal transfer frequency

Figure 4 shows MTF as a function of (a) TiO_2 content, (b) SiO_2 content and (c) CaF_2 content at three welding current levels. The overall MTF was calculated as the average of ten individual measurements, applying the same analytical approach as employed in [13, 14, 16]. An individual MTF measurement was performed by counting the number of droplets within randomly selected 200-ms intervals from a 3.2-second high-speed video. Error bars represent the standard deviation of these measurements, calculated using "STDEV.S" function in Excel.

As shown in this figure, the MTF increased with rising welding current across all wires. Notably, the influence of

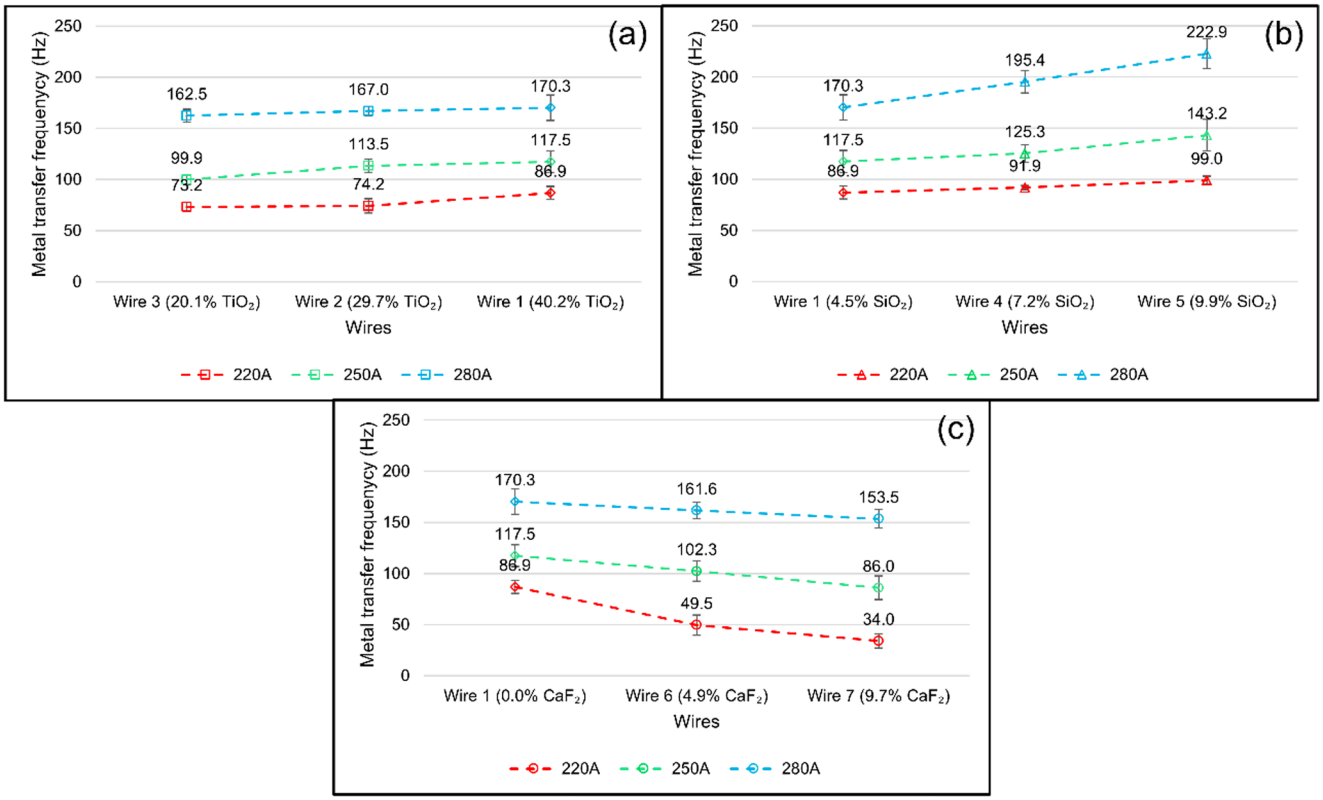

Fig. 4 Metal transfer frequency as a function of (**a**) TiO_2 content, (**b**) SiO_2 content and (**c**) CaF_2 content at three welding current levels

flux composition on MTF varied distinctly with changes in TiO_2, SiO_2 and CaF_2 contents. An increasing tendency was observed for the wires with increases in TiO_2 and SiO_2 contents, while added CaF_2 component represented an opposite tendency.

Figure 4(a) demonstrates a slight increase in the MTF with rising TiO_2 content. At low current, the MTF increased from 73.2 Hz ± 4.6 Hz to 86.9 Hz ± 6.3 Hz as TiO_2 content rose from 20.1% to 40.2%. A similar trend was observed at medium current, where the MTF increased from 99.9 Hz ± 5.2 Hz to 117.5 Hz ± 10.7 Hz. However, at high current, the effect of TiO_2 content was less pronounced, with the MTF rising only modestly from 162.5 Hz ± 6.3 Hz to 170.3 Hz ± 12.5 Hz.

Figure 4(b) illustrates a more pronounced increase in the MTF with rising SiO_2 content compared to TiO_2, particularly at a high current level. At low and medium currents, the MTF increased within the ranges of 86.9 Hz ± 6.3 Hz to 99.0 Hz ± 3.9 Hz and 117.5 Hz ± 10.7 Hz to 143.2 Hz ± 15.5 Hz as the SiO_2 content rose from 4.5% to 9.9%, respectively. The MTF showed a steeper rise, climbing from 170.3 Hz ± 12.5 Hz to 222.9 Hz ± 14.7 Hz at high current.

Figure 4(c) shows that increasing CaF_2 content consistently reduced the MTF across all current levels. The effect was most obvious at a low current, where the MTF decreased dramatically from 86.9 Hz ± 6.3 Hz to 34.0 Hz ± 7.0 Hz when the CaF_2 content increased from 0 to 9.7%. At medium current, the MTF decreased from 117.5 Hz ± 10.7 Hz to 86.0 Hz ± 11.6 Hz. A similar, though less significant, decline was observed from 170.3 Hz ± 12.5 Hz to 153.5 Hz ± 9.1 Hz at high current.

Figure 5 illustrates the equivalent DD as a function of (a) TiO_2 content, (b) SiO_2 content and (c) CaF_2 content at three welding current levels. In this study, we assumed that the melting rate of the wire was the product of WFS (v_{wfs}) and wire cross-sectional area (S_w), and the droplets were spherical [20]. Based on the calculated MTF (f), the volume of a droplet (V) can be estimated as follows:

$$V = \frac{v_{wfs} S_w}{f} \tag{1}$$

From V, the equivalent DD (d) could be deduced as the equation below:

$$d = \sqrt[3]{\frac{6 \times V}{\pi}} \tag{2}$$

Error bars represent the standard deviation of these measurements, processed in the same way as the MTF.

The results show that at all current levels, DD decreased with increasing TiO_2 and SiO_2 contents, while the higher

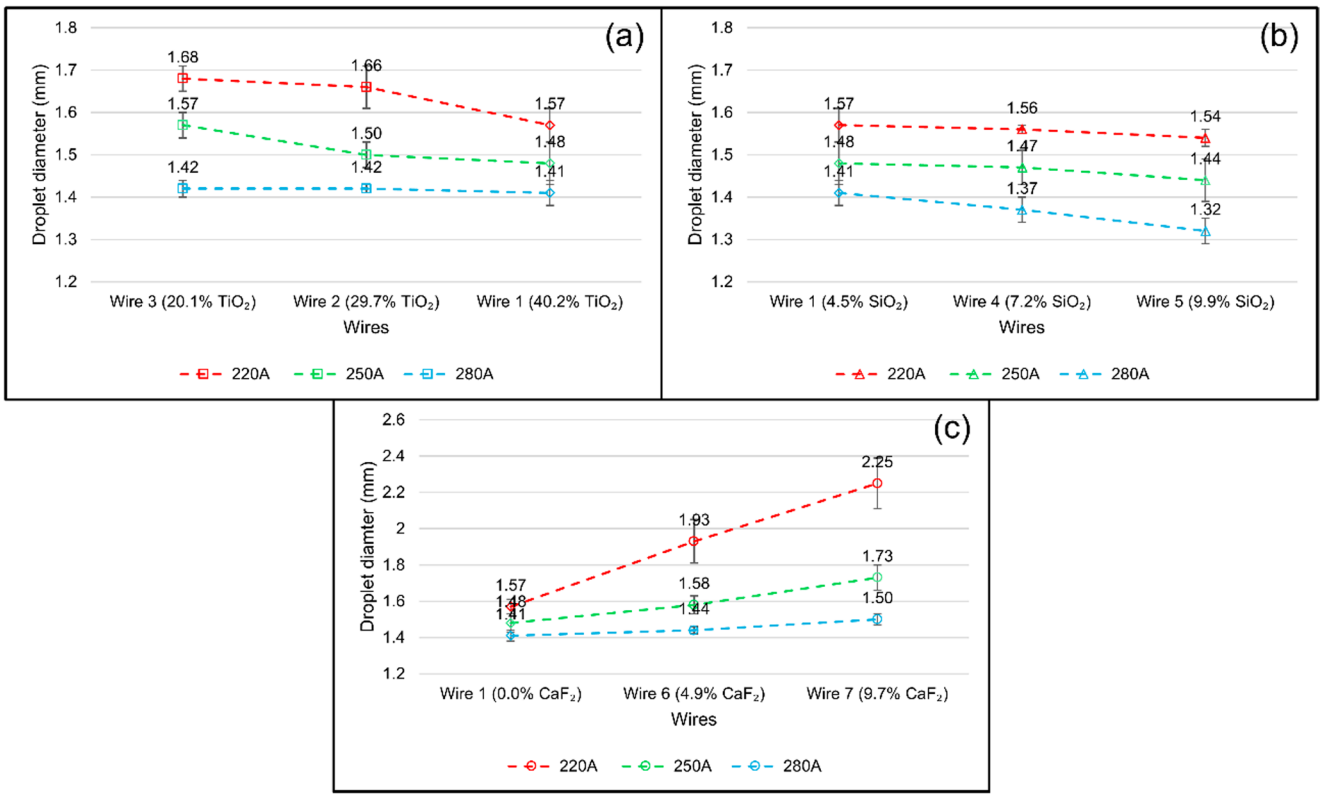

Fig. 5 Equivalent droplet diameter as a function of (**a**) TiO_2 content, (**b**) SiO_2 content and (**c**) CaF_2 content at three welding current levels

CaF_2 content generated a larger droplet. For TiO_2 wires, DD decreased from 1.68 mm ± 0.03 mm to 1.57 mm ± 0.04 mm at 220 A, from 1.57 mm ± 0.03 mm to 1.48 mm ± 0.05 mm at 250 A, and remained nearly constant at approximately 1.42 mm ± 0.02 mm at 280 A. In the case of SiO_2 wires, DD gradually decreased from 1.57 mm ± 0.04 mm to 1.54 mm ± 0.02 mm at 220 A, from 1.48 mm ± 0.05 mm to 1.44 mm ± 0.05 mm at 250 A, and from 1.41 mm ± 0.03 mm to 1.32 mm ± 0.03 mm at 280 A. In contrast, wires with increasing CaF_2 content exhibited a gradual increase in DD. They rose from 1.57 mm ± 0.04 mm to 2.25 mm ± 0.14 mm at 220 A, 1.48 mm ± 0.05 mm to 1.73 mm ± 0.07 mm at 250 A, and 1.41 mm ± 0.03 mm to 1.50 mm ± 0.03 mm at 280 A.

3.2 Metal transfer behavior and arc appearance

To better understand how the flux composition affects metal transfer characteristics in rutile-type FCAW, this section presents synchronized high-speed images of the arc and metal transfer. The analysis includes time-sequential images of metal transfer and arc appearance for all experimental wires at a medium current. Their typical images at three welding current levels are also presented. Drawing on the arc plasma distribution analysis by Trinh et al. [13, 14] and Le et al. [16], we delineated two characteristic plasma regions within the arc: a gas-plasma region (indicated by the blue dashed line) and a metal-plasma region (indicated by the orange one). Notably, the flux column (where the flux core has not melted completely) existed for all wires regardless of welding currents.

Figure 6 presents time-sequential images during one cycle of metal transfer for (a) Wire 3 (20.1% TiO_2), (b) Wire 2 (29.7% TiO_2) and (c) Wire 1 (40.2% TiO_2) at 250 A. Notably, all figures below correspond to FCAW conducted under Ar-20% CO_2 shielding gas. As shown, increasing the TiO_2 content from 20.1% to 40.2% led to a shorter droplet detachment duration (from 11.6 ms to 8.4 ms, respectively). The nearly close detachment durations of Wire 1 (8.4 ms) and Wire 2 (8.6 ms) aligned well with their corresponding MTF reported earlier in Fig. 4(a).

In case of TiO_2 wires, the droplet morphology exhibited negligible variation, with the droplet remaining well-confined throughout its growth prior to detachment. The droplet consistently formed and detached away from the wire center, regardless of TiO_2 content. DD was larger for Wire 3, while it remained relatively similar for Wires 1 and 2. The characteristics are consistent with DD presented earlier in Fig. 5(a).

The arc appearance of TiO_2 wires was also examined. In all cases, gas plasma was maintained near the wire tip during droplet growth, while metal plasma was located at the

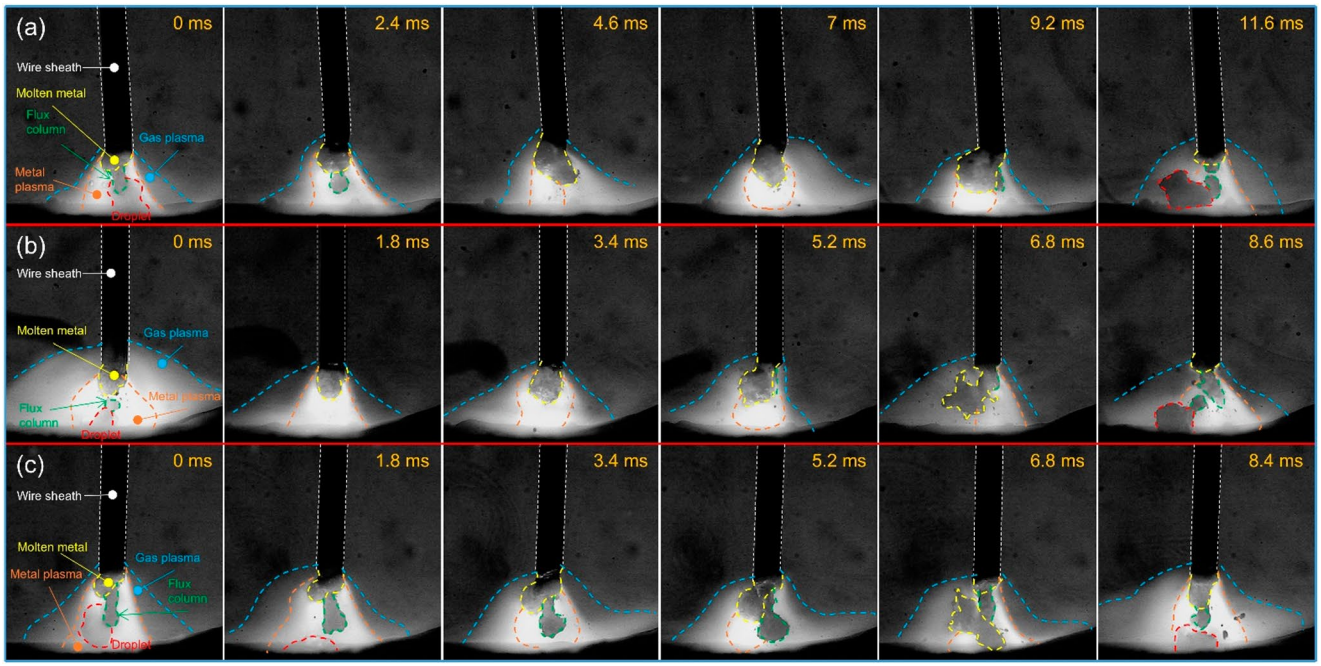

Fig. 6 Time-sequential images during one cycle of metal transfer for (**a**) Wire 3 (20.1% TiO_2), (**b**) Wire 2 (29.7% TiO_2) and (**c**) Wire 1 (40.2% TiO_2) at 250 A in FCAW

arc core and gradually shifted downward along the surface of the droplet (at 9.2 ms in Fig. 6(a) and at 5.2 ms in Fig. 6(b, c)). Additionally, the brightness of the metal plasma was observed to be similar for all TiO_2 wires.

Figure 7 depicts typical images of metal transfer behavior and arc appearance for wires with varying TiO_2 content at (a) 220 A, (b) 250 A, and (c) 280 A in FCAW. The results showed that DD decreased with increasing current. At low and medium current levels, the droplet tended to be away from the wire center, whereas it was located on the central axis with a flux column passing through it at high current. These metal transfer behaviors were in good agreements with findings in [16].

As shown in Fig. 7, the gas plasma appearances were similar to those shown in Fig. 6 at all currents. The metal plasma attachment shifted from under the droplet to the region near the wire tip as the current increased. The metal plasma gradually covered the higher part of the droplet with increasing current during the droplet's growth, regardless of TiO_2 content.

Figure 8 shows time-sequential images during one cycle of metal transfer for (a) Wire 1 (4.5% SiO_2), (b) Wire 4 (7.2% SiO_2) and (c) Wire 5 (9.9% SiO_2) at 250 A in FCAW. The images suggested that the detachment time decreased from 8.4 ms to 6.4 ms with increasing SiO_2 content. However, the difference between Wire 1 and Wire 4 was minimal (8.4 ms vs. 8.0 ms). Like TiO_2 cases, the droplet morphologies for SiO_2 cases were away from the wire center. The difference was that the droplet became more elongated when SiO_2 content increased. Notably, the droplet appeared to flow downward along the flux column during its growth at the highest SiO_2 level, before detaching.

The figure also depicts that both gas and metal plasmas were initially located near the wire tip at the moment of droplet detachment. For all SiO_2 cases, the gas plasma consistently maintained its position near the wire tip. In contrast, the metal plasma shifted to the region under the bottom of the droplet during the droplet's growth, which was observed at 5.2 ms for Wire 1 and 3.2 ms for Wire 4, while the metal plasma remained near the wire tip for Wire 5.

Figure 9 illustrates typical images of metal transfer behavior and arc appearance for wires with varying SiO_2 content at (a) 220 A, (b) 250 A, and (c) 280 A in FCAW. As the welding current increased, the droplet morphology changed from a large DD to a smaller DD (with an elongated formation). The position of the droplet during its growth in SiO_2 wires followed a similar trend to that observed in TiO_2 wires; it shifted from an off-center location to the region that was aligned with the wire center. Additionally, the arc appearance for SiO_2 wires mirrored that of the TiO_2 wires as the current increased.

Figure 10 shows time-sequential images during one cycle of metal transfer for (a) Wire 1 (without CaF_2), (b) Wire 6 (4.9% CaF_2) and (c) Wire 7 (9.7% CaF_2) at 250 A in FCAW. As the CaF_2 content increased from 0 to 9.7%, the detachment duration lasted from 8.4 ms to 13.8 ms, respectively. This increased duration was accompanied by a noticeable increase in DD. The droplets remained away from wire

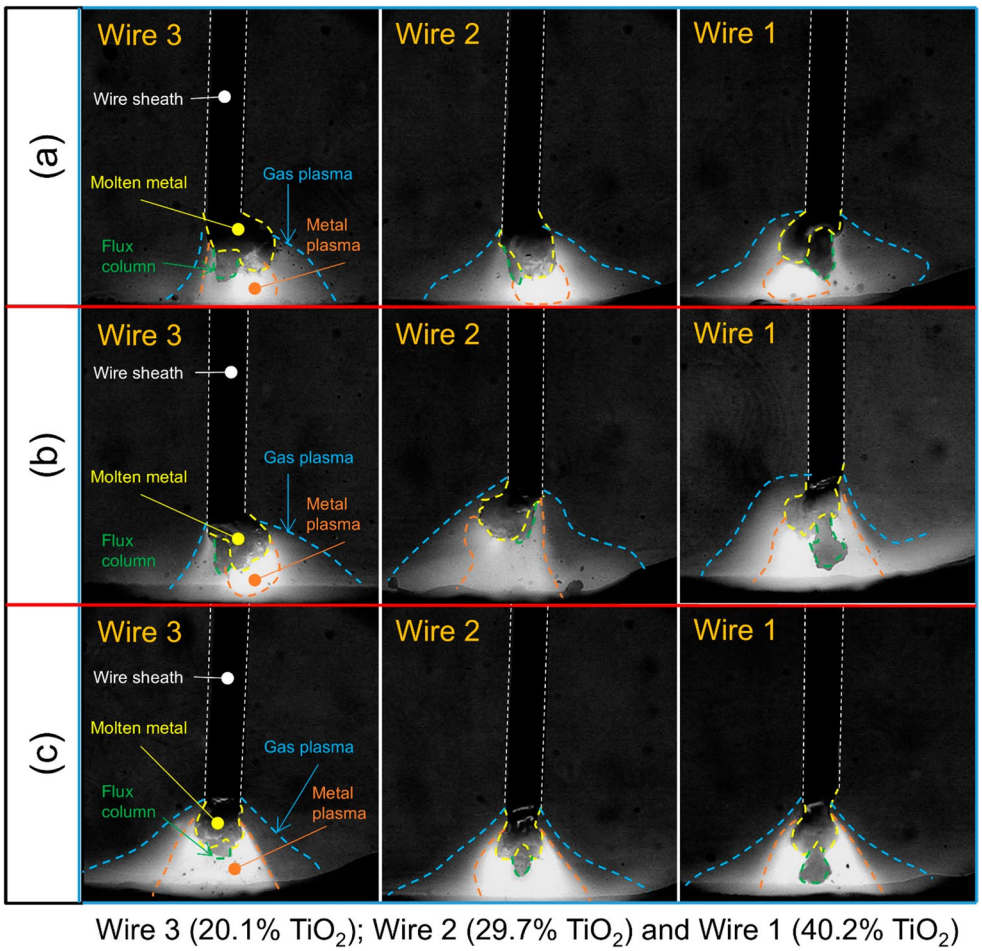

Fig. 7 Typical images of metal transfer behavior and arc appearance for the wires with different TiO_2 contents at (**a**) 220 A, (**b**) 250 A and (**c**) 280 A in FCAW

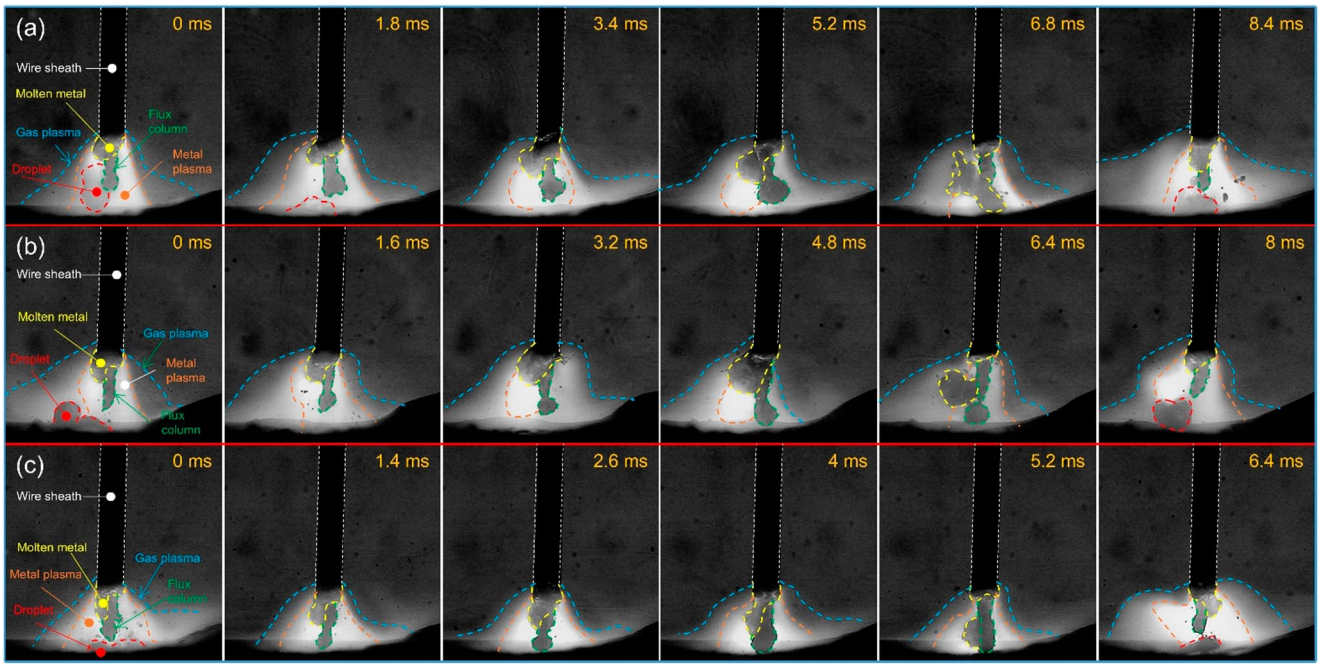

Fig. 8 Time-sequential images during one cycle of metal transfer for (**a**) Wire 1 (4.5% SiO_2), (**b**) Wire 4 (7.2% SiO_2) and (**c**) Wire 5 (9.9% SiO_2) at 250 A in FCAW

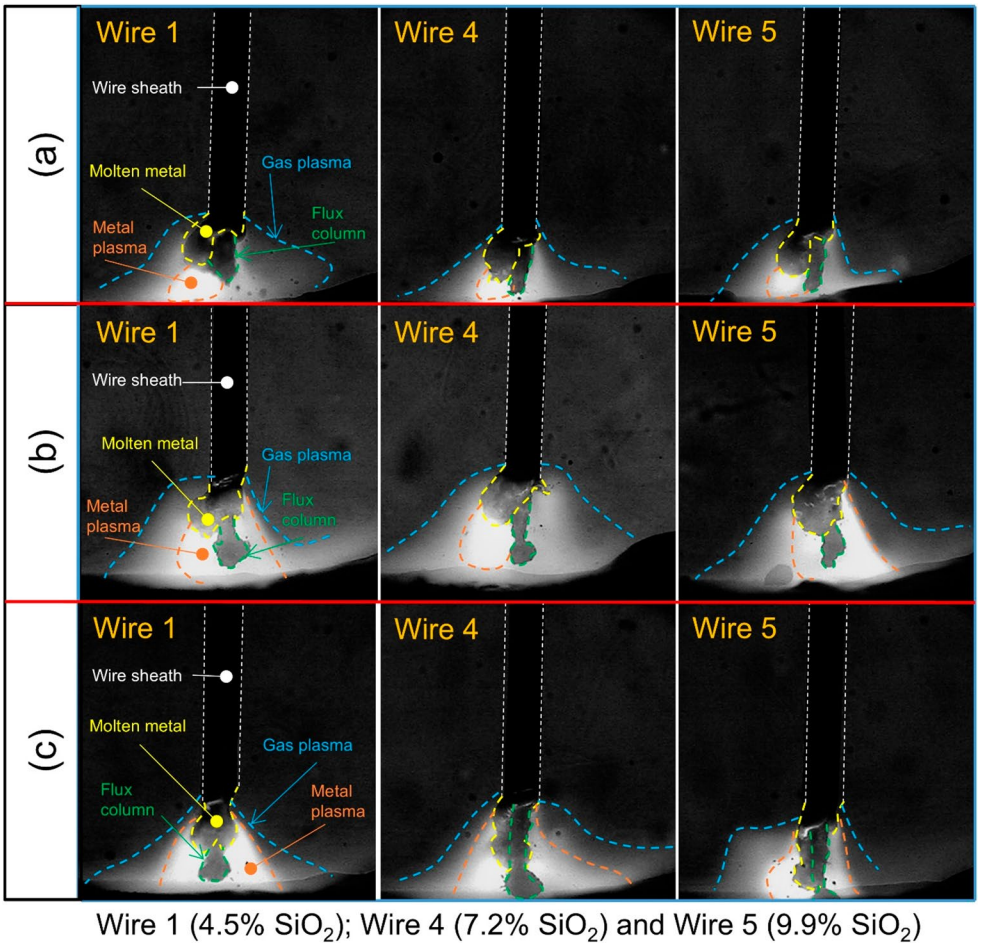

Fig. 9 Typical images of metal transfer behavior and arc appearance for the wires with different SiO_2 contents at (**a**) 220 A, (**b**) 250 A and (**c**) 280 A in FCAW

center regardless of CaF_2 content. Notably, the droplet was observed to be pushed slightly upward during its growth (6.6 ms for Wire 6 and 5.6 ms for Wire 7).

As shown in Fig. 10, the gas plasma remained concentrated near the wire tip across all CaF_2 wires. In contrast, the metal plasma was positioned under the bottom of the molten droplet. Moreover, the region of metal plasma appeared to be broader and brighter as CaF_2 content increased.

Figure 11 displays typical images of metal transfer behavior and arc appearance for the wires with different CaF_2 contents at (a) 220 A, (b) 250 A and (c) 280 A in FCAW. Across all current levels, DD increased with increasing CaF_2 content. At low current, the droplet was gradually pushed upward (repelled transfer). When the welding current increased (particularly at high current), this behavior became less pronounced. At low current, the arc attachment was located on the lower part of the molten droplet for Wires 6 and 7. As the current increased, the arc attachment shifted progressively toward the wire tip, regardless of CaF_2 content. Additionally, metal plasma attachment was mainly located under the bottom of droplets at low and medium currents, while it shifted to the middle part of droplets at high current.

Variations in metal transfer behavior induced by different flux compositions are expected to influence weld bead microstructure, dilution, and penetration. While these properties are essential for assessing overall weld performance and would offer valuable complementary insight, their evaluation requires dedicated analysis of weld pool heat transfer, fluid flow, and solidification phenomena. As the present study is intentionally confined to arc-droplet interactions prior to weld pool formation, these aspects fall beyond its current scope. Future work will therefore aim to establish a direct correlation between metal transfer characteristics and weld bead geometry as well as microstructural evolution.

4 Discussion

This section considers how flux composition influences metal transfer characteristics (MTF and DD) in rutile-type FCAW, based on the experimental findings presented in the previous section. As in Eqs. 1 and 2, DD is proportional to the WFS divided by the MTF. The former depends primarily on energy balance, and the latter on force balance.

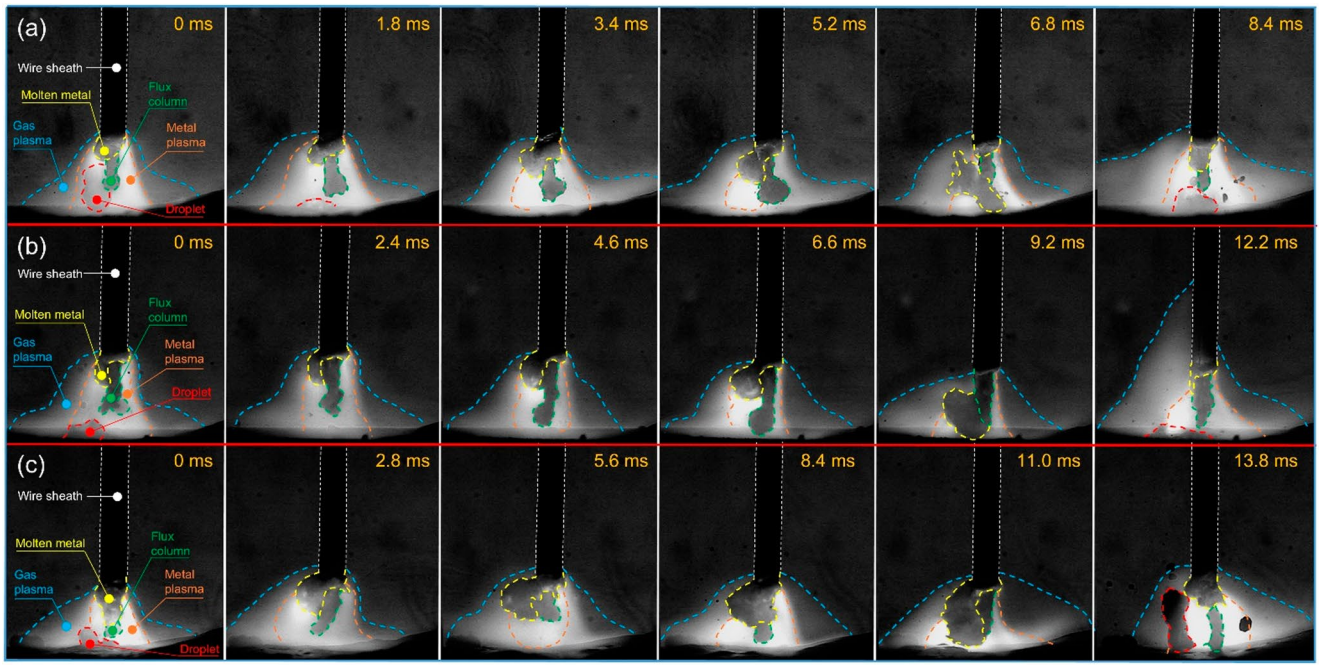

Fig. 10 Time-sequential images during one cycle of metal transfer for (**a**) Wire 1 (without CaF_2), (**b**) Wire 6 (4.9% CaF_2) and (**c**) Wire 7 (9.7% CaF_2) at 250 A in FCAW

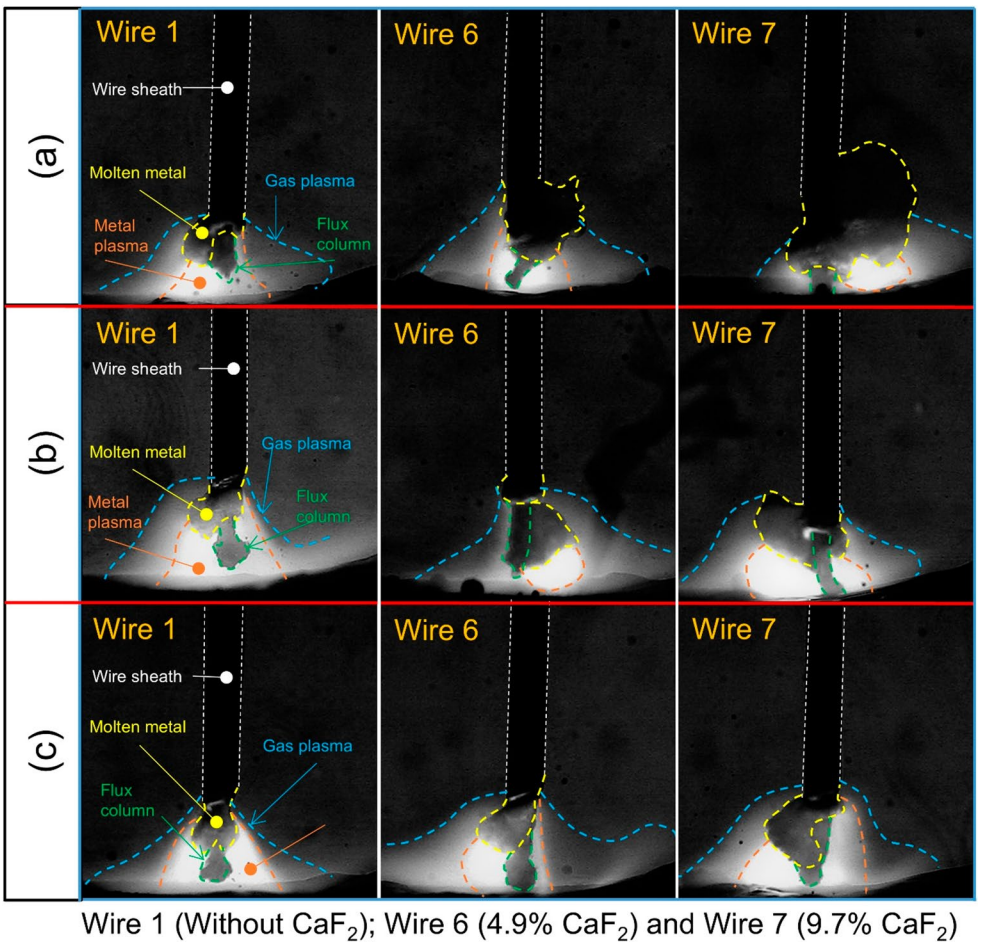

Fig. 11 Typical images of metal transfer behavior and arc appearance for the wires with different CaF_2 contents at (**a**) 220 A, (**b**) 250 A and (**c**) 280 A in FCAW

First, the energy balance is considered. As discussed in [16, 21], the WFS is chosen to maintain a constant arc voltage, and is primarily determined by the melting rate of the metal sheath. However, at high arc voltage, the arc current decreased due to the increased resistance of the high arc length. To achieve the target I_{out}, a higher I_{set} was therefore required, resulting in a very high WFS, especially in case of CaF_2 content. TiO_2 (the main component of rutile wire) has a very low electrical conductivity compared to iron (a wire sheath component). Thus, most of the welding current is concentrated in the sheath. As a result, the Joule heating and heating related to electron absorption into the anode wire are significantly concentrated within this region. Therefore, the sheath melted faster than the flux core, leading to the formation of an extended flux column [21].

Figure 2 showed that the decrease in WFS with increasing iron content followed a smoother trend. In this study, WFS is automatically determined by the equipment using I_{set} (see Sect. 2.1). Below, we will consider why this value appeared to depend on the flux composition from the perspective of electrical resistivity and melting rate. The change in TiO_2, SiO_2 and CaF_2 contents was accompanied by a change in iron content in the flux. This change occurred to maintain a constant flux ratio. The change in melting rate might be related to the iron content in the flux. Matsuda et al. [22]. studied metal transfer and arc characteristics of 1.6 mm titania-based flux core wires with varying iron powder content ratios in flux and measured wire resistance at room temperature using an Impedance-Bridge Meter. Their results indicated that increasing the iron powder content ratios in flux from 0 to 100% reduces the wire resistance from 14.0 to 11.9 μΩ mm. It means that the electrical conductivity of the flux increased. The increase in electrical conductivity of flux led to the decrease in the current passing through the sheath metal. As a result, the WFS was reduced. Referring to Table 1, the iron content tended to decrease when TiO_2, SiO_2, and CaF_2 components were added to the flux. Consequently, WFS depended on the iron content in the wire almost independently of the TiO_2, SiO_2, and CaF_2 contents, increasing linearly with current.

Next, the force balance is considered. In GMAW with a solid wire, several key forces act on droplets: surface tension, arc pressure, drag force, gravity, and the Lorentz force [23]. Among these, the surface tension and arc pressure are upward forces that hinder droplet detachment. The arc pressure is generated by the Lorentz force within the arc, and it increases when the current path is concentrated directly under the bottom of the droplet. The drag force acts downward as friction between the molten droplet and the surrounding plasma flow. This force is typically negligible due to its small magnitude. Gravity, also a downward force, plays a more significant role at low current levels. The Lorentz force, whose direction and magnitude depend on the current path within the droplet, can vary: if the current path expands downward in a cone shape, the Lorentz force acts both downward and inward; if the path is strictly vertical, it acts only inward. The current path itself is determined by the electrical conductivity distribution of the arc plasma surrounding the droplet and the morphology of the droplet. At low currents, the main factors affecting droplet detachment are the arc pressure and gravity.

In this study, two distinct hypotheses are proposed to explain the influence of flux composition on metal transfer characteristics. The first is the effect of recoil pressure (vapor pressure) generated by the vaporization of TiO_2, SiO_2 and CaF_2 components. In laser keyhole welding, intense heating at the laser focal point on the weld pool surface rapidly vaporizes the metal as the temperature approaches its boiling point. The resulting recoil pressure depresses the weld pool surface, creating a keyhole [24]. In FCAW, the droplet is pushed upward by a similar effect [16]. The magnitude of the recoil pressure will be estimated later. The second suggests that variations in flux additives such as TiO_2 and SiO_2 influence the magnitude of surface tension, thereby affecting the metal transfer behavior.

Now, the former hypothesis is considered. In GMAW, surface tension (in the order of 1000 N m^{-2}) and gravity are the two main factors affecting droplet detachment at low current levels [23]. The detachment occurs when the magnitude of gravity exceeds the surface tension. In FCAW, volatile elements in the flux can produce excessive vaporization, introducing an additional retaining force (recoil pressure) acting on the bottom of the droplets [16]. Le et al. [16] reported that increasing sodium content in flux generated more sodium vapor in the arc plasma. This vaporization produced a strong recoil pressure acting on the bottom of droplet. When the vaporization was sufficiently high, the recoil pressure became the dominant factor affecting droplet detachment. Based on qualitative findings about metal transfer behavior and arc appearance as shown in Fig. 11 and **Sect. 3.2**, it is possible to expect that the same effect of recoil pressure will occur for CaF_2 wires.

The primary purpose of adding CaF_2 into the flux is to reduce the hydrogen and oxygen contents in the welding process. In FCAW, moisture on the workpiece surface or inside flux core is the main source of hydrogen. Increasing CaF_2 content is thought to enhance the vaporization, which intensifies the recoil pressure. This recoil pressure pushed droplets upward to a higher position, hindering droplet detachment (Fig. 11(a)), increasing the detachment time, thereby reducing MTF and producing the larger droplets.

As the current increases, the Lorentz force, which is proportional to the square of the current, increases steeply. Thus, the dominant factor in droplet detachment is the Lorentz

force at high currents, rather than retaining forces (such as surface tension and recoil pressure) at low currents. At high currents, the arc attachment expanded toward the wire tip rather than remaining under the bottom of the droplet, as seen at low currents. Combined with the strong Lorentz force, this expansion enhanced neck formation. This made droplet detachment faster under the pinch effect. In FCAW, the Lorentz force is further intensified by the increased current density in the wire sheath at high currents. At the same time, the arc expansion reduced the current flowing directly under the bottom of the droplet. This phenomenon lowered the arc pressure under the droplet. Consequently, the droplet was pushed upward less strongly, allowing the MTF to increase with current. Nonetheless, the recoil pressure continued to affect the overall trend of MTF in CaF_2 wires. As a result, the MTF decreased, and the DD was larger as the CaF_2 content increased.

It is instructive to compare recoil pressures arising from vaporization of TiO_2, SiO_2, and CaF_2. Wu and Wahlbeck [25] measured vapor pressures of TiO(g) and TiO_2(g) over TiO_2(s)-Ti_2O_3(s) two-phase solids using Knudsen Effusion Mass Spectrometry (KEMS) [25–31]. This method derives vapor pressure from mass loss under vacuum and molecular flow conditions, which ensure near-equilibrium vaporization. In contrast, the FCAW arc plasma is strongly non-equilibrium and ionizing, and gas composition depends on kinetics, ionization, and local oxygen supply. Therefore, the present recoil pressure assessment aims only at a relative comparison of gaseous species from TiO_2, SiO_2, and CaF_2.

Due to the limitations of the available vaporization temperature range in KEMS [29]: the temperature of 2000 K is chosen for comparison in this study. Wu and Wahlbeck [25] reported a p_{TiO}/p_{TiO_2} ratio of 4.06, indicating dominant TiO(g) vaporization. At 2000 K, the p_{TiO} is ~ 2.38×10^{-2} N m^{-2} (2.35×10^{-7} atm) reported by Wu and Wahlbeck [25] and that of ~ 0.08 N m^{-2} reported by Stolyarova et al. [26].

Shornikov et al. [27] reported that above 1800 K, under chemically neutral or near-neutral conditions, the vapor over silicon dioxide is dominated by (SiO), (O), and (O_2). At 2000 K, the p_{SiO} was reported as ~ 1.00 N m^{-2} (1.00×10^{-5} atm) by Shornikov et al. [27] and ~ 2.34 N m^{-2} (2.30×10^{-5} atm) by Schick [28].

For CaF_2, we estimated by using Clausius – Clapeyron equation as followings:

$$P_{VAP} = P_{ATM} exp\left[\frac{-H_V M_B}{R}\left(\frac{1}{T_m} - \frac{1}{T_{mB}}\right)\right] \quad (3)$$

Where M_B is the atomic weight of iron, H_V is the heat of vaporization, R is the ideal gas constant, P_{VAP} is the vapor pressure of liquid metal calculated by the Clausius-Clapeyron equation, P_{ATM} is the atmo-spheric pressure, T_m and T_{mB} are the temperature of droplet (2000 K) and the boiling temperature of CaF_2, respectively.

The calculated vapor pressure at 2000 K was 6.46×10^4 N m^{-2}, compared with reported values of ~5×10^2 N m^{-2} (~ 5×10^{-3} atm) from Blue et al. [30], and Schulz and Searcy [31].

As a result, CaF_2 exhibits a dominant vapor pressure, approximately two orders of magnitude higher than that of TiO_2 and SiO_2, thereby exerting a pronounced influence on metal transfer behavior. Under these conditions, the recoil pressure generated by CaF_2 exceeds the stabilizing effect of surface tension (shown above), leading to a fundamental modification of the metal transfer mechanism for CaF_2-containing wires. Consistent with this trend, Le et al. [16] reported that recoil pressure increases with alkali content. Accordingly, high CaF_2 contents generate strong recoil pressures, promoting repelled metal transfer, as illustrated in Figs. 10 and 11.

Another possible mechanism is that the high specific heat of CaF_2 vapor enhances arc constriction, thereby increasing arc pressure beneath the droplet and hindering detachment, which results in repelled metal transfer, particularly for Wire 7 in Fig. 11(a). A similar effect is well established for CO_2 additions to argon shielding gas, where the high specific heat and molecular nature of CO_2 promote arc constriction [13, 23]. Consistently, increasing CaF_2 content led to pronounced arc constriction (Figs. 10 and 11), suggesting an analogous mechanism. To quantify this effect, numerical simulations of the specific heat of CaF_2, Ar-20% CO_2 (MAG) gas, and iron plasmas were conducted.

Figure 12 showed the dependence of specific heat of CaF_2, Ar-20%CO_2 shielding gas, and Fe plasmas on temperature. The shielding gas mixture data was obtained using the methods described in [32, 33], while the iron data were taken from [34]. The specific heat of CaF_2 plasmas was calculated assuming Local Thermodynamic Equilibrium (LTE) using the methods outlined in [35]. The partition functions for Ca, Ca^+, Ca^{2+}, Ca^{3+}, Ca^{4+}, F, F^+, F^{2+}, and F^{3+} were calculated using the atomic energy levels from the National Institute of Standards and Technology (NIST) Atomic Spectra Database [36]. Thermodynamic data for F_2, F^-, CaF and CaF_2 were taken from the JANAF Table [37].

Previous studies have shown that FCAW plasma comprises a metal plasma beneath the molten metal and a surrounding gas plasma [13, 14, 16]. Numerical simulations for MCAW by Tashiro et al. [21]. reported metal plasma temperature of ~ 6000 K and that of ~ 12,000 K for gas plasma. These values are generally considered comparable to those in GMAW; therefore, for simplicity, the metal and gas plasma temperatures in FCAW are assumed to be similar to those in MCAW and GMAW. At these temperatures, the calculated specific heats are 6400.0 J kg^{-1} K^{-1} for CaF_2

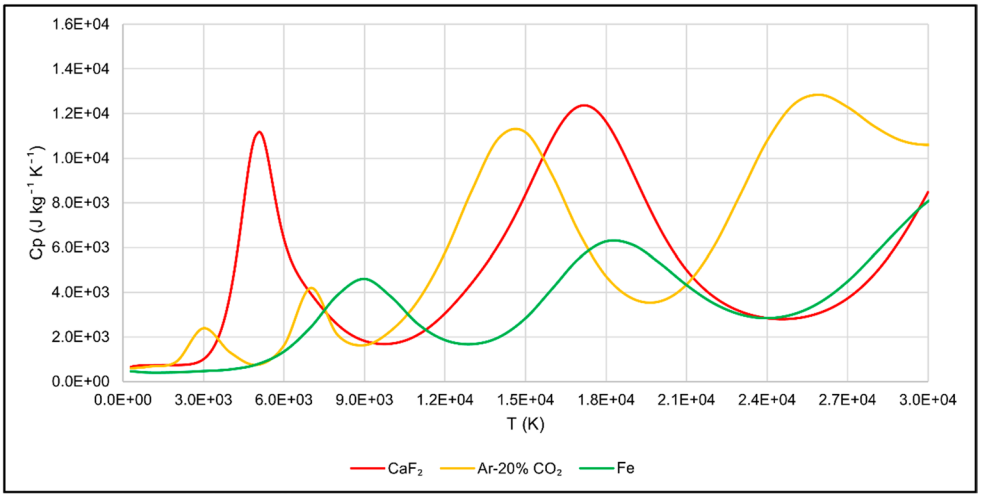

Fig. 12 Dependence of specific heat of CaF_2, Ar-20%CO_2 shielding gas, and Fe plasmas on temperature

plasma, and 1342.9 J kg^{-1} K^{-1} for iron plasma at 6000 K, and 5764.9 J kg^{-1} K^{-1} for MAG gas plasma at 12,000 K.

In solid-wire GMAW, the central arc is generally dominated by iron vapor [23, 38]. To isolate the effect of CaF_2 vapor specific heat on metal transfer, two limiting cases were considered: a central arc composed entirely of iron vapor, and one composed entirely of CaF_2 vapor, the latter representing the high-CaF_2 condition (e.g., Wire 7 with 9.7% CaF_2 in the flux). The surrounding gas plasma was assumed to have identical properties in both cases. Based on the calculated results, complete replacement of iron vapor by CaF_2 vapor in the metal plasma increased the specific heat by approximately a factor of 4.8, attributable to the triatomic nature of CaF_2 and its high dissociation energy. Consequently, CaF_2 vapor is expected to induce stronger arc constriction than iron vapor, thereby increasing arc pressure and suppressing droplet detachment, analogous to the behavior observed in CO_2 arc welding, which may promote repelled transfer in high-CaF_2-containing wires, as seen in Fig. 11.

The recoil pressures from TiO_2 and SiO_2 are almost negligible, so their effect can be ignored. Another mechanism is therefore required to explain the influence of TiO_2 and SiO_2.

Next, the second hypothesis, related to surface tension, is discussed. Based on the analysis of the metal transfer behavior of TiO_2 and SiO_2 wires through the high-speed images, it was found that the droplet morphology for TiO_2 wires remained well-confined, while elongated droplets were observed for SiO_2 wires. These characteristics have not previously been reported and need further investigation. However, a possible explanation is related to the surface tension. This factor is also considered to lead to a higher MTF for SiO_2 wires compared to TiO_2 wires.

The surface tension of weld pool is influenced by oxygen originating from oxides [11]. When oxides generate sufficient oxygen within weld pool, it tends to reduce the surface tension. The oxygen released in the weld pool may result from chemical reactions between molten slag and metal [39]. A similar process is expected in molten droplets. The following formula qualitatively explains how flux additives regulate oxygen content in droplets [39].

$$\log[\%O] = -\frac{A}{n}B_L - \frac{m}{n}\log[\%M] + \frac{1}{n}\log(\%M_mO_n) - \frac{1}{n}(C - nD) \quad (4)$$

where [%O] denotes the oxygen content in a molten droplet and B_L indicates the slag basicity. The contents of alloy elements in the molten droplets and the deoxidation products in the welding slag are represented by [%M] and ($\%M_mO_n$), respectively. $AB_L + C$ expresses the logarithm of the equilibrium index, defined as $(\%M_mO_n)/[\%M]^m(\%FeO)^n$ in molten droplets, while D is the logarithm of the oxygen distribution index, represented by [%O]/(%FeO) in molten droplets.

Equation 4 shows the factors that influence the oxygen content in molten droplets. The influence of basicity in the first term will be discussed later. The second and third terms represent the effects of alloy elements and deoxidation products, respectively decreasing and increasing the oxygen content in droplets, indicating that higher TiO_2 and SiO_2 contents can raise the oxygen content and reduce droplet surface tension. In this study, the last term (C - *n*D) is omitted for simplicity, as the balance between ($\%M_mO_n$) and [%M] in the equilibrium index is too complex to evaluate. Since the aim is only to assess qualitatively the effect of oxide formation on released oxygen content, the logarithm of the oxygen distribution index by [%O]/(%FeO) is also ignored. The qualitative effect of slag basicity in the first term is discussed using the formula below [40].

$$B_L = \frac{CaO + CaF_2 + MgO + K_2O + Na_2O + Li_2O + 1/2(MnO + FeO)}{SiO_2 + 1/2(Al_2O_3 + TiO_2 + ZrO_2)} \quad (5)$$

From Eq. 5, when assuming other components remaining constant, higher CaF_2 content increased slag basicity.

Substituting it into Eq. 4 showed that oxygen content in droplets decreased, raising the surface tension. The combined effect of the strong recoil pressure explained above and the high surface tension suppressed droplet detachment, which lowered the MTF as CaF_2 content increased. Conversely, higher TiO_2 and SiO_2 contents reduced slag basicity. The oxygen content in the droplets then rose, surface tension decreased, and the MTF increased, as shown in Fig. 4. Equation 5 also indicates that only half as much added TiO_2 as SiO_2 is required to reduce the basicity by a given factor. Thus, SiO_2 likely influenced droplet surface tension more strongly than TiO_2, though further confirmation is needed.

Moreover, oxides with lower melting points decompose more readily under the heat of the welding arc. The Ellingham diagram presented in [15] illustrates the standard free energy of oxidation reactions as a function of temperature for a specified oxygen partial pressure. Each line indicates the thermodynamic stability field of a metal and its corresponding oxide. Regions above a line (where the standard free energy is higher) indicate conditions favoring oxide stability, whereas regions below the line correspond to conditions under which the unoxidized metal is thermodynamically more stable. TiO_2, with a higher melting point ($1738°C$) and a lower Ellingham line compared to SiO_2 ($1600°C$), is a more stable oxide. Therefore, TiO_2 releases less oxygen into the weld pool, resulting in a smaller reduction in surface tension than SiO_2 [11]. With similar properties to the weld pool, molten droplets can be influenced by the same effect. Furthermore, the lower surface tension can facilitate the pinch effect on the droplet.

In Active Tungsten Inert Gas Welding (A-TIGW), the surface of the workpiece is coated by a thin layer of powder consisting of inorganic compounds such as B_2O_3, TiO_2, SiO_2 and MgO before welding. For stainless steel 304 L as a workpiece, the layer of these molten fluxes reduces the surface tension of the molten pool. It also changes the temperature coefficient from negative to positive and alters the Marangoni convection [11]. As a result, the penetration depth in A-TIGW increases. An assumption is that the coating density (the mass per unit surface area of oxides) for both TiO_2 and SiO_2 is around 1.76 mg cm^{-2}, which is the same value used in [11] for A-TIGW with arc time from 5 to 25 s. According to experimental data, Li et al. [11] reported that the averaged value of surface tension of molten metal in a stable stage with SiO_2 powder was lower than with TiO_2 ($\sim$ 0.88 N m^{-1} compared to $\sim$ 0.96 N m^{-1}, respectively). Note that the unit of the values was corrected from mN m^{-1} in the original text to N m^{-1}. Furthermore, Liu et al. [41] showed that SiO_2 has a lower surface tension of 295 mN m^{-1} than that of 338 mN m^{-1} for TiO_2 at same temperature of $1400°C$ (1673 K). As a result, droplets formed on SiO_2 wires moved downward along the flux column and detached more easily than those formed on TiO_2 wires. Consequently, SiO_2 wires showed higher MTF than TiO_2 wires.

Finally, the relationship between the WFS, MTF, and DD is discussed. The discussion focuses on the influence of flux compositions (CaF_2, SiO_2 and TiO_2) under the same welding current. CaF_2 wires produced the highest WFS, but the MTF was the lowest because of the high recoil pressure. The molten volume grew greatly and detached as droplets with larger DD in the repelled transfer mode, indicating that the detachment force was not enough to detach the droplet frequently and compensate for the high WFS. In contrast, SiO_2 wires exhibited a higher MTF due to the balance of forces, but the WFS was lower. This resulted in smaller DD. For TiO_2 wires, the WFS stayed almost constant, as shown in Fig. 2. The force balance also changed a little because the addition of TiO_2 had only minor influences on the recoil pressure and surface tension. As a result, the MTF increased only slightly with TiO_2 content. This might explain a slight variation in DD for TiO_2 wires.

Thus, the DD depended more strongly on the MTF than the WFS under differing flux compositions, so that the DD was inversely proportional to the MTF. Consequently, DD depended significantly on the flux composition due to variations in the physical properties.

Figure 13 summarizes explanations of the effect of (a) TiO_2, (b) SiO_2 and (c) CaF_2 on metal transfer behavior in FCAW. In Fig. 13(a), for TiO_2 wires, the droplet morphology remained well-confined shape and deviated toward the flux column. The gas plasma was attached near the wire tip, while the metal plasma was centered on the middle part of the droplet. Here, stronger surface tension hindered detachment, which occurred only when gravity overcame this force. In contrast, Fig. 13(b) shows the elongated droplet resulting from the low surface tension of the droplet. This droplet flowed gradually along the flux column and detached at its tip under the pinch effect. Gas plasma remained near the wire tip, with metal plasma enveloping the elongated droplet. Figure 13(c) illustrates CaF_2 wires, where the strong recoil pressure pushed a larger molten droplet upward. In this case, gas plasma shifted to the middle of the droplet, while metal plasma was located under it.

5 Conclusion

This study investigates the influence of flux composition on metal transfer behavior in rutile-type Flux-Cored Arc Welding (FCAW). Using high-speed video analysis, the metal transfer characteristics, such as Metal Transfer Frequency (MTF) and droplet diameter (DD), and the arc appearance of seven flux core wires with varying TiO_2, SiO_2, and CaF_2

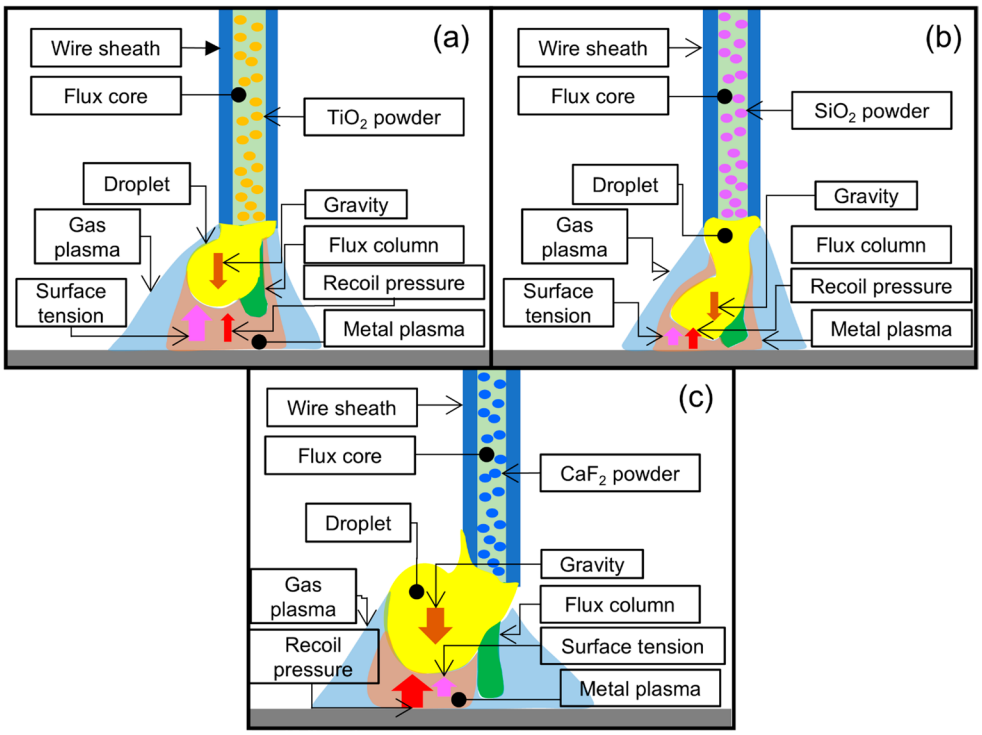

Fig. 13 Schematics of explanation on effect of (**a**) TiO_2, (**b**) SiO_2 and (**c**) CaF_2 on metal transfer behavior in FCAW

contents in flux were examined. The tests were conducted at three welding currents of 220, 250 and 280 A with Ar-20%CO_2 shielding gas. The key findings are summarized as follows:

1. The iron content in flux composition primarily governed the Wire Feed Speed (WFS), where a higher content lowered the wire resistance to decrease the WFS.
2. An increase in CaF_2 content in the flux reduced the MTF dramatically from 86.9 Hz $\pm$ 6.3 Hz to 34.0 Hz $\pm$ 7.0 Hz at 220 A, whereas it generally increased with increasing TiO_2 and SiO_2 contents.
3. The vaporization from CaF_2 generates a recoil pressure far exceeding that of TiO_2 and SiO_2, which acts upward on the droplet and inhibits detachment. This effect intensifies with increasing CaF_2 content, particularly at lower currents, leading to a reduced MTF. At higher currents, the influence of recoil pressure weakens, resulting in smaller MTF differences among wires with varying CaF_2 contents. Another possibility is the high specific heat of CaF_2 plasma likely enhances arc constriction and arc pressure, further suppressing droplet detachment and promoting repelled transfer in high-CaF_2-containing wires.
4. In wires containing TiO_2, the MTF showed a slight increase with TiO_2 content in the range of 162.5–170.3 Hz at 280 A, while in the wires containing SiO_2, the MTF exhibited a large increase with SiO_2 content, from 170.3 Hz to 222.9 Hz, at the same current.
5. The great increase in MTF with SiO_2 content was attributed to increasing oxygen in droplets through slag-metal reactions, leading to a lower surface tension, because of the lower basicity of SiO_2 than TiO_2.
6. The DD depended strongly on the MTF rather than the WFS under differing flux compositions, so that the DD was inversely proportional to the MTF. Consequently, it was concluded that the DD depended on flux composition due to variations in the physical properties.

The research has elucidated how the flux compositions of additives such as TiO_2, SiO_2, and CaF_2 affect the metal transfer in rutile-type FCAW. The findings give helpful information for manufacturers to design better flux core wires that improve welding efficiency, productivity, and quality.

Acknowledgements Not applicable.

Author contributions Dang Khoi Le: investigation, visualization, writing–original draft preparation.
Shinichi Tashiro: conceptualization, writing–review and editing,
Kieu Anh Duong Nguyen: investigation, visualization.
Quang Ngoc Trinh: investigation, visualization.
Tetsuo Suga: project administration.
Naoki Sawamura: resources, validation.
Kazuhiro Fukuda: resources, validation.
Shuji Sasakura: resources, validation.
Patricio Fernando Mendez: supervision, writing–review and editing.
Anthony B. Murphy: supervision, writing–review and editing.
Van Hanh Bui: supervision, writing–review and editing.
Manabu Tanaka: supervision, writing–review and editing.
All authors have read and agreed to submit the current version of the manuscript.

Funding Open Access funding provided by The University of Osaka. This work was supported by JSPS KAKENHI (Grant Number JP25K08344), the Project on Design & Engineering by Joint Inverse Innovation for Materials Architecture (DEJI2MA) from the Ministry of Education, Culture, Sports, Science and Technology (MEXT), and an OU Master Plan Implementation Project promoted under Osaka University.

Data availability Data can be available based on the requirements to verify this work.

Declarations

Competing interests The authors declare no competing interests.

References

1. Brien AO (1987) Welding Handbook. Macmillan Education UK, London
2. Yu J, Cho SM (2017) Metal-cored welding wire for minimizing weld porosity of zinc-coated steel. J Mater Process Tech 249:350–357. https://doi.org/10.1016/j.jmatprotec.2017.06.012
3. French IE, Bosworth MR (1995) A comparison of pulsed and conventional welding with basic flux cored and metal cored welding wires. Weld Res supplement 74(6):197s–205s
4. Holly S, Mayer P, Bernhard C, Posch G (2019) Slag characterization of 308L-type stainless steel rutile flux-cored wires. Weld world 63:293–311. https://doi.org/10.1007/s40194-018-0675-6
5. Widgery D (1994) Tubular wire welding. Woodhead, Cambridge
6. Izutani S, Shimizu H, Suzuki K, Koshiishi F, Hirata Y (2006) Observation and Classification of Droplet Transfer in Gas Metal Arc Welding. In: IIW commission XII
7. Liu S, Siewert TA (1989) Metal transfer in gas metal arc welding: Droplet rate. Weld Res supplement 68(2):52s–58s
8. Bauné E, Bonnet C, Liu S (2013) Assessing metal transfer stability and spatter severity in flux cored arc welding. Sci Technol Weld Joining 6(3):139–148. https://doi.org/10.1179/136217101101538677
9. Mendez PF, Jenkins NT, Eagar TW (2000) Effect of electrode droplet size on evaporation and fume generation in GMAW. Proceedings of the Gas Metal Arc Welding for the 21st Century Conference, Orlando
10. Haidar J (1999) An analysis of heat transfer and fume production in gas metal arc welding. III. J Appl Phys 85(7):3448. https://doi.org/10.1063/1.370500
11. Li C, Shi Y, Gu Y, Yang F (2017) Effects of oxide on surface tension of molten metal. RSC Adv 7(85):53941–53950. https://doi.org/10.1039/C7RA11185A
12. Kim YS, Eagar TW (1993) Analysis of metal transfer in gas metal arc welding. Weld Res supplement 72(6):269s–278s
13. Trinh NQ, Le KD, Tashiro T, Suga T, Sasakura S, Fukuda K, Murphy AB, Bui HV, Tanaka M (2024) Optimization of metal transfer in rutile flux-cored arc welding through controlled CO_2 concentration in argon-CO_2 shielding gas. J Manuf Process 124:590–603. https://doi.org/10.1016/j.jmapro.2024.06.047
14. Trinh NQ, Tashiro S, Tanaka K, Suga T, Kakizaki T, Yamazaki K, Morimoto T, Shimizu H, Lersvanichkool A, Murphy AB, Bui GV, Tanaka M (2021) Effects of alkaline elements on the metal transfer behavior in meta cored arc welding. J Manuf Process 68:1448–1457. https://doi.org/10.1016/j.jmapro.2021.06.061
15. Valensi F, Pellerin N, Pellerin S, Castillon Q, Dzierzega K, Briand F, Planckaert JP (2018) Influence of Wire Initial Composition on Anode Microstructure and on Metal Transfer Mode in GMAW: Noteworthy Role of Alkali Elements. Plasma Chem Plasma Process 38:177–205. https://doi.org/10.1007/s11090-017-9860-4
16. Le DK, Tashiro S, Trinh QN, Suga T, Naoki S, Fukuda K, Sasakura S, Alvarez-Rocha JE, Mendez PF, Murphy AB, Bui VH, Tanaka M (2025) Elucidation of alkali element's role in optimizing metal transfer behavior in rutile-type flux-cored arc welding. J Manuf Process 139:105–125. https://doi.org/10.1016/j.jmapro.2025.02.021
17. Bang K, Jung H, Han I (2010) Comparison of the Effects of Fluorides in Rutile-Type Flux Cored Wire. Met Mater Int 16(3):489–494. https://doi.org/10.1007/s12540-010-0622-6
18. Kil W, Shin M, Bang K (2017) Effects of Fluoride in the Flux on Hydrogen Content in Weld Metal and Operating Behavior in FCAW-S. J Weld Join 35(5):65–70. https://doi.org/10.5781/JWJ.2017.35.5.9
19. Matsushita M (2018) Hydrogen control in steel weld metal by means of fluoride additions in welding flux. Dissertation, Colorado School of Mines
20. Trinh NQ, Tashiro S, Suga T, Kakizaki T, Yamazaki K, Lersvanichkool A, Bui HV, Tanaka M (2022) Metal transfer behavior of metal-cored arc welding in pure argon shielding gas. Metals 12(1577). https://doi.org/10.3390/met12101577
21. Tashiro S, Trinh QN, Le DK, Suga T, Kakizaki T, Yamazaki K, Murphy AB, Lersvanichkool A, Bui VH, Tanaka M (2024) Elucidation of droplet detachment mechanism in metal-cored arc welding. J Manuf Process 124:1583–1605. https://doi.org/10.1016/j.jmapro.2024.07.040
22. Matsuda F, Ushio M, Tatsuo T, Toshihiko M (1980) Arc Characteristics and Metal Transfer for Flux-cored Electrode in GMA Welding (Report II) (Welding Physics, Processes & Instruments). Trans JWRI 9(1):39–46. http://hdl.handle.net/11094/4076
23. Ogino Y, Hirata Y (2015) Numerical simulation of GMA metal transfer phenomena including arc plasma. Proc Jpn Weld Soc 33:1–12. https://doi.org/10.2207/qjjws.33.1
24. Allmen MV, Blatter A (1995) Laser-Beam Interactions with Materials. Springer-, Berlin Heidelberg, New York
25. Wu HY, Wahlbeck PG (1972) Vapor Pressures of TiO(g) in Equilibrium with Ti_2O_3(s) and Ti_3O_5(s, β); Dissociation Energy of TiO(g). J Chem Phys 56:4534–4540. https://doi.org/10.1063/1.1677900
26. Stolyarova VL, Shilov AL, Vorozhtcov VA, Lopatin SI, Fedorova AV (2025) High-temperature mass spectrometric study and modeling of thermodynamic properties in the La_2O_3-TiO_2 system. Chem Thermodyn Therm Anal 18:100164. https://doi.org/10.1016/j.ctta.2025.100164
27. Shornikov SI, Archakov IY, Shul'ts MM (1998) Mass Spectrometric Study of Vaporization and Thermodynamic Properties of Silicon Dioxide. I. Composition of the Gas Phase and Partial Vapor Pressures of the Molecular Forms over Silicon Dioxide. Russ J Gen Chem 68(8):1171–1177 Translated from Zhurnal Obshchei Khimii 68(8):1233–1240

28. Schick HL (1960) A thermodynamic analysis of the high-temperature vaporization properties of silica. Chem Rev 60(4):331–362. https://pubs.acs.org/doi/abs/ https://doi.org/10.1021/cr60206a002
29. Stolyarova VL, Seetharaman S, Svard D, Semenov GA (1998) A high-temperature mass spectrometric study of the vaporization processes of fluxes based on CaO-$CaCl_2$ and CaO-CaF_2 systems. Rapid Commun Mass Spectrom 12:1335–1343. https://doi.org/10.1002/(SICI)1097-0231(19981015)12:19%3C1335::AID-RCM295%3E3.0.CO;2-H
30. Blue GD, Green JW, Bautista RG, Margrave JL (1963) The sublimation pressure of calcium(II) fluoride and the dissociation energy of calcium(I) fluoride. J Phys Chem 67(4):877–882. https://doi.org/10.1021/j100798a039
31. Schulz DA, Searcy A (1963) Vapor pressure and heat of sublimation of calcium fluoride. J Phys Chem 67(1):103–106. https://doi.org/10.1021/j100795a023
32. Murphy AB, Arundell CJ (1994) Transport coefficients of argon, nitrogen, oxygen, argon-nitrogen and argon-oxygen plasma. Plasma Chem Plasma Process 14:451–490. https://doi.org/10.1007/BF01570207
33. Murphy AB (1995) Transport coefficients of air, argon-air, nitrogen-air, and oxygen-air plasma. Plasma Chem Plasma Process 15:279–307. https://doi.org/10.1007/BF01459700
34. Murphy AB (2010) The effects of metal vapor in arc welding. J Phys D Appl Phys 43:43400. https://iopscience.iop.org/article/ https://doi.org/10.1088/0022-3727/43/43/434001
35. Murphy AB, Tam E (2014) Thermodynamic properties and transport coefficients of arc lamp plasmas: argon, krypton and xenon. J Phys D: Appl Phys 47:295202. https://doi.org/10.1088/0022-3727/47/29/295202
36. Kramida A, Ralchenko Y, Reader J, NIST ASD Team (2024) NIST Atomic Spectra Database, version 5.12. https://physics.nist.gov/asd. National Institute of StandardsTechnology, Gaithersburg, MD. https://doi.org/10.18434/T4W30F
37. Chase MW Jr (ed) (1998) NIST–JANAF thermochemical tables, 4th ed., J. Phys. Chem. Ref. Data, Monograph 9, pp 703–736
38. Schnick M, Füssel U, Hertel M, Spille-Kohoff A, Murphy AB (2010) Metal vapour causes a central minimum in arc temperature in gas-metal arc welding through increased radiative emission. J Phys D Appl Phys 43(2):022001. https://doi.org/10.1088/0022-3727/43/2/022001
39. Kasamatsu Y (1962) Physico-Chemical Study on the Chemical Reaction between Molten Slag and Metal in Welding Process (Report 5). J Japanese Weld Soc 31(9):775–781
40. Fan J, Zhang J, Zhang D (2024) Thermodynamic Insights into the Influence of Welding Current on Oxygen Levels in the Submerged Arc Welding Process. Processes 12:2147. https://doi.org/10.3390/pr12102147
41. Liu Y, Lv X, Bai C, Yu B (2014) Surface Tension of the Molten Blast Furnace Slag Bearing TiO_2: Measurement and Evaluation. ISIJ Int 54(10):2154–2161. https://doi.org/10.2355/isijinternational.54.2154